Near-field Fourier transform polarimetry by use of a discrete space-variant subwavelength grating

Gabriel Biener, Avi Niv, Vladimir Kleiner, and Erez Hasman

Optical Engineering Laboratory, Faculty of Mechanical Engineering, Technion–Israel Institute of Technology, Haifa, Israel 32000

Received February 18, 2003; revised manuscript received May 15, 2003; accepted May 28, 2003

We present a unique method for real-time polarization measurement by use of a discrete space-variant subwavelength grating. The formation of the grating is done by discrete orientation of the local subwavelength grooves. The complete polarization analysis of the incident beam is determined by spatial Fourier transform of the near-field intensity distribution transmitted through the discrete subwavelength dielectric grating followed by a subwavelength metal polarizer. We discuss a theoretical analysis based on Stokes–Mueller formalism, as well as on Jones calculus, and experimentally demonstrate our approach with polarization measurements of infrared radiation at a wavelength of 10.6 μm. © 2003 Optical Society of America

OCIS codes: 260.5430, 050.2770, 050.1960, 230.5440.

1. INTRODUCTION

Optical polarimetry measurement has been widely used for a large range of applications such as ellipsometry,[1] bioimaging,[2] imaging polarimetry,[3] and optical communications.[4] A commonly used method is the measuring of the time-dependent signal once the beam is transmitted through a photoelastic modulator[5] or a rotating quarter-wave plate (QWP) followed by an analyzer.[6] The polarization state of the beam can be derived by Fourier analysis of the detected signal. This method, however, requires a sequence of consecutive measurements, thus making it impractical for real-time polarization measurement in an application such as adaptive polarization-mode dispersion compensation in optical communications. Moreover, it involves either mechanically or electronically active elements, resulting in a complicated and cumbersome device.

An increasing demand for faster and simpler methods has led to the development of the simultaneously four-channel ellipsometer.[7] In this method the beam is split into four channels; each is analyzed by using different polarization optics, while the real-time polarization state is calculated from the measured intensities. The main drawback of this method is its high sensitivity to statistical errors as a result of the low number of measurements. Recently, Gori[8] proposed real-time polarimetry by use of a space-variant polarizer, in what is basically a manifestation of the four-channel technique. This method relies on measuring the far-field intensity and therefore is not suitable for on-chip integrated applications.

In our recent letter,[9] we presented a space-domain analogy to the rotating QWP method. In this method spatial intensity distribution analysis is applied for real-time near-field polarimetry. The intensity modulation is achieved by a space-variant wave plate, realized as a computer-generated space-variant continuous subwavelength grating, followed by an analyzer. However, continuity of the subwavelength grating had led to a space-dependent local period. Therefore, in order for the period not to exceed the Wood anomaly,[9,10] the elements were restricted in their physical dimensions. Moreover, the varying periodicity had complicated the optimization of the photolithographic process and had led to spatial variations in the retardation of the element.

In this paper we propose real-time near-field polarimetry by spatial discrete rotating of the groove orientation of a subwavelength dielectric grating. The grating of this type of element is divided into equal-sized zones. The subwavelength grooves are of uniform orientation and period at each zone and are rotated at discrete angles respective to each zone. The resulting elements are unlimited in their dimensions and have uniform optical parameters. We named such elements discrete space-variant subwavelength dielectric gratings (DSGs). Unlike the case for other methods based on Fourier analysis, no active elements are required to determine the polarization state of an incident beam. Our method is less sensitive to statistical errors because of the increased number of measurements, and it is suitable for real-time applications and can be used in compact configurations. It is possible to integrate our polarimeter on a two-dimensional detector array for laboratory on-chip applications to achieve a high-throughput and low-cost commercial polarimeter for biosensing.

In Section 2 we discuss a theoretical analysis of the near-field intensity distributions of the beams transmitted through our computer-generated space-variant subwavelength gratings as a function of the polarization state of the incident beams by use of Stokes–Mueller formalism. In Appendix A we use Jones calculus to gain physical insight into the main results of Section 2. In Section 3 we describe the realization procedure and ex-

perimentally demonstrate the ability of our method to measure the polarization state as well as the degree of polarization for fully and partially polarized light. Section 4 is devoted to concluding remarks.

2. THEORETICAL ANALYSIS BY USE OF STOKES–MUELLER FORMALISM

The concept of near-field polarimetry based on subwavelength gratings is presented in Fig. 1. A uniformly polarized light is incident upon a polarization-sensitive medium (e.g., biological tissue, optical fiber, wave plate, etc.) and then transmitted through a DSG, which acts as a space-variant wave plate, followed by a polarizer. The resulting intensity distribution is imaged onto a camera and captured for further analysis. It will show further that the emerging intensity distribution is uniquely related to the polarization state of the incoming beam. This dependence is given by a spatial Fourier series analysis, whereby the resulting Fourier coefficients completely determine the polarization state of the incoming beam.

The DSGs are considered wave plates with constant retardation and space-variant fast axes, the orientation of which is denoted by $\theta(x, y)$. It is convenient to form such space-variant wave plates by use of a subwavelength grating. When the period of a subwavelength periodic structure is smaller than the incident wavelength, only the zero order is a propagating order, and all other orders are evanescent. The subwavelength periodic structure behaves as a uniaxial crystal with the optical axes parallel and perpendicular to the subwavelength grooves.[11] Therefore, by fabricating quasi-periodic subwavelength structures, for which the orientation of the subwavelength grooves is changed along the length of the element, one can form space-variant wave plates.

The creation of a DSG is done by discrete orientation of the local subwavelength grating, as illustrated in Fig. 2(a). The DSG is obtained by dividing the element into N equal-sized zones along the x axis, where each zone consists of a uniform orientation as well as a uniform subwavelength grating period. The orientation of the grooves is defined by the angle θ between the grating vector K_g of the subwavelength grating (perpendicular to the grooves) and the x axis; therefore θ is a function of the x coordinate $[\theta(x)]$. The grating period d is defined as the distance between the nearest zones having identical orientations. We consider the period of grating d as larger than the incident wavelength λ, whereby the local subwavelength period of the grooves, Λ, is smaller than the incident wavelength. Figure 2(a) presents a DSG with a period that consists of $N = 4$ zones of uniform orientation of the subwavelength grating. We denote N as the number of discrete levels.

The polarization state within the Stokes representation is described by a Stokes vector $\mathbf{S} = (S_0, S_1, S_2, S_3)^{\mathrm{T}}$, where S_0 is the intensity of the beam, whereas S_1, S_2, and S_3 represent the polarization state. In general, ${S_0}^2 \geqslant {S_1}^2 + {S_2}^2 + {S_3}^2$, where the equality holds for fully polarized beams.[6] The polarization state emerging from an optical system (i.e., wave plates, polarizers, etc.) is linearly related to the incoming polarization state through $\mathbf{S}' = \mathbf{MS}$, where $\mathbf{M}$ is a 4×4 real Mueller matrix of the system and $\mathbf{S}$ and $\mathbf{S}'$ are the Stokes vectors of the incoming and outgoing polarization states, respectively.

The optical system under consideration consists of a DSG followed by a polarizer. This composite element can be described, in Cartesian coordinates, by the Mueller matrix

$$\mathbf{M} = \mathbf{PR}(-\theta)\mathbf{WR}(\theta), \tag{1}$$

where

$$\mathbf{R}(\theta) = \begin{bmatrix} 1 & 0 & 0 & 0 \\ 0 & \cos(2\theta) & \sin(2\theta) & 0 \\ 0 & -\sin(2\theta) & \cos(2\theta) & 0 \\ 0 & 0 & 0 & 1 \end{bmatrix}$$

is the Mueller matrix that represents rotation of the axis frame by angle θ and

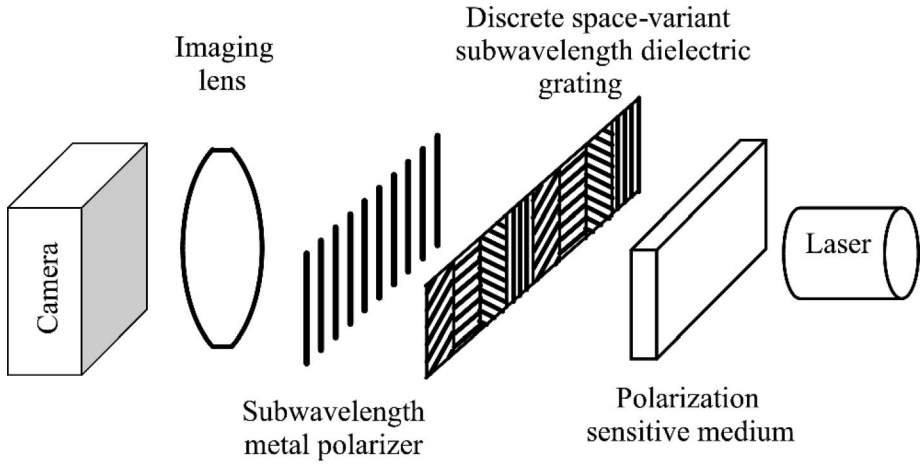

Fig. 1. Schematic presentation of near-field Fourier transform polarimetry based on a discrete space-variant subwavelength dielectric grating followed by a subwavelength metal polarizer.

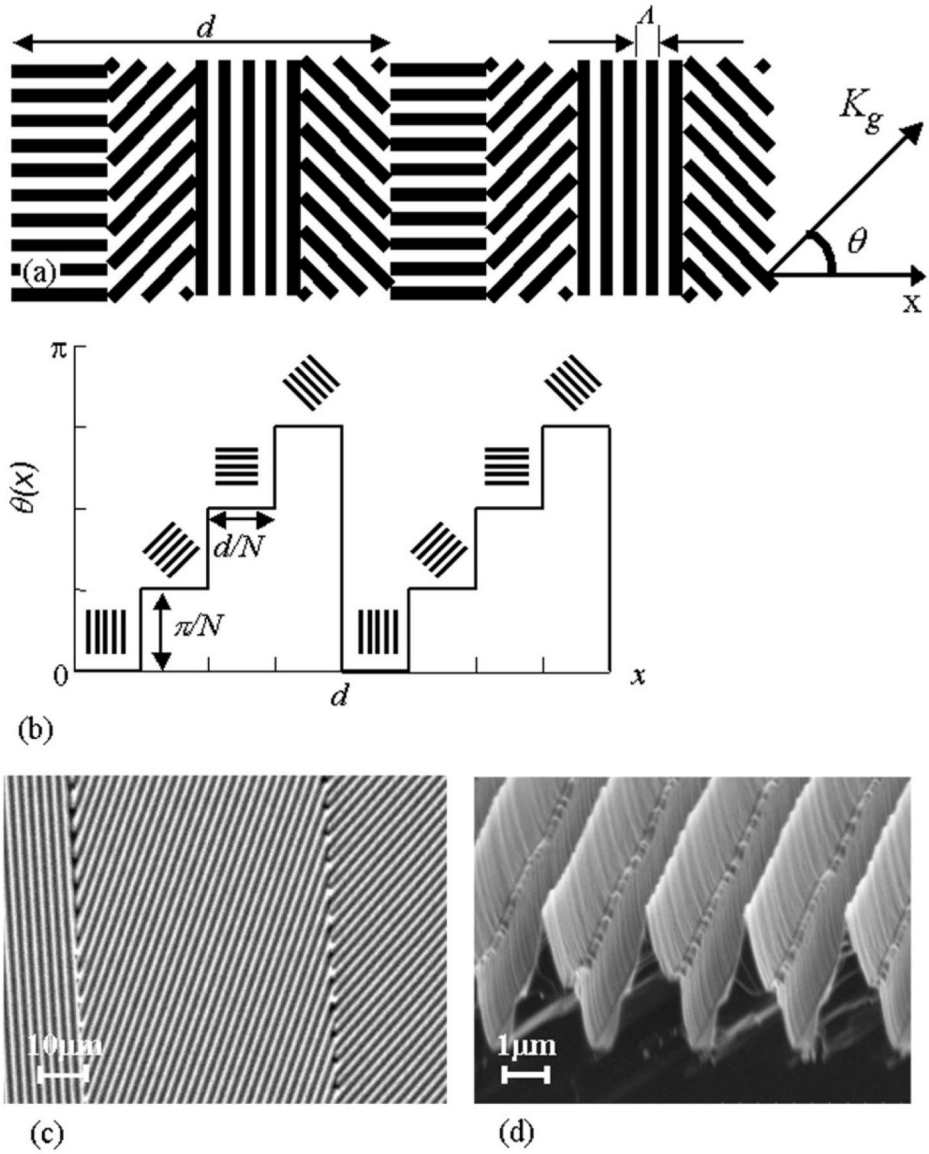

Fig. 2. (a) Magnified geometry of the discrete space-variant dielectric grating with a number of discrete levels $N = 4$. (b) Discrete rotation angle of the subwavelength grating as a function of x coordinate; the local groove orientations are indicated. (c) Scanning electron microscopy image of a region on the subwavelength structure. (d) Scanning electron microscopy image of a cross section of the subwavelength grooves.

$$\mathbf{W} = \frac{1}{2}\begin{bmatrix} t_x^2 + t_y^2 & t_x^2 - t_y^2 & 0 & 0 \\ t_x^2 - t_y^2 & t_x^2 + t_y^2 & 0 & 0 \\ 0 & 0 & 2t_x t_y \cos\phi & -2t_x t_y \sin\phi \\ 0 & 0 & 2t_x t_y \sin\phi & 2t_x t_y \cos\phi \end{bmatrix}$$

is the Mueller matrix of a transversally uniform retarder[6] with retardation ϕ and real transmission coefficients for two eigenpolarizations t_x and t_y. Finally,

$$\mathbf{P} = \frac{1}{2}\begin{bmatrix} 1 & 1 & 0 & 0 \\ 1 & 1 & 0 & 0 \\ 0 & 0 & 0 & 0 \\ 0 & 0 & 0 & 0 \end{bmatrix}$$

is the Mueller matrix of an ideal horizontal polarizer.

The outgoing intensity can be related to the incoming polarization state of the beam by calculating the Mueller matrix given by Eq. (1) and using the linear relation between the incoming and outgoing Stokes vectors, yielding

$$\begin{aligned} S_0'(x) = {} & \tfrac{1}{4}(AS_0 + \tfrac{1}{2}(A + C)S_1 + B(S_1 + S_0)\cos[2\theta(x)] \\ & + (BS_2 - DS_3)\sin[2\theta(x)] + \tfrac{1}{2}(A - C) \\ & \times \{S_1 \cos[4\theta(x)] + S_2 \sin[4\theta(x)]\}), \end{aligned} \tag{2}$$

where $A = t_x^2 + t_y^2$, $B = t_x^2 - t_y^2$, $C = 2t_x t_y \cos\phi$, and $D = 2t_x t_y \sin\phi$.

Equation (2) describes the intensity of the outgoing beam as a truncated Fourier series with coefficients that depend on the Stokes parameters of the incident beam. In our case θ represents the discrete rotation angle of the

retarder (subwavelength grating) as a function of the location along the x axis. A single period of θ can be written explicitly as

$$\theta(x) = \begin{Bmatrix} 0, & 0 < x < \dfrac{d}{N} \\ \dfrac{\pi}{N}, & \dfrac{d}{N} < x < \dfrac{2d}{N} \\ \vdots & \vdots \\ \dfrac{\pi(m-1)}{N}, & \dfrac{d(m-1)}{N} < x < \dfrac{dm}{N} \\ \vdots & \vdots \\ \dfrac{\pi(N-1)}{N}, & \dfrac{d(N-1)}{N} < x < d \end{Bmatrix}, \tag{3}$$

where m is an integer number, with $N \geqslant m \geqslant 0$. Figure 2(b) illustrates $\theta(x)$ for a number of discrete levels $N = 4$. Note that $\theta(x)$ is periodic in π.

Inserting the discrete angle described by Eq. (3) into Eq. (2) and then expanding the trigonometric expressions into a Fourier series yields the resulting intensity distribution

$$\begin{aligned} 4S_0'(x) = {} & AS_0 + \frac{1}{2}(A + C)S_1 + B(S_1 + S_0) \\ & \times \sum_{n=1}^{\infty} [a_n \cos(2\pi nx/d) + b_n \sin(2\pi nx/d)] \\ & + (BS_2 - DS_3) \sum_{n=1}^{\infty} [c_n \sin(2\pi nx/d) \\ & + d_n \cos(2\pi nx/d)] + \frac{1}{2}(A - C) \\ & \times \left\{ S_1 \sum_{n=1}^{\infty} [e_n \cos(4\pi nx/d) + f_n \sin(4\pi nx/d)] \right. \\ & + S_2 \sum_{n=1}^{\infty} [g_n \sin(4\pi nx/d) \\ & \left. + h_n \cos(4\pi nx/d)] \right\}. \end{aligned} \tag{4}$$

The corresponding Fourier coefficients in Eq. (4) are given by

$$\begin{aligned} a_n &= c_n = \frac{N}{2\pi n} \sin\left(\frac{2\pi}{N}\right), \\ b_n &= d_n = \frac{N}{\pi n} \sin^2\left(\frac{\pi}{N}\right), \\ e_n &= g_n = \frac{N}{4\pi n} \sin\left(\frac{4\pi}{N}\right), \\ f_n &= h_n = \frac{N}{2\pi n} \sin^2\left(\frac{2\pi}{N}\right) \end{aligned} \tag{5}$$

for $n = kN \pm 1$ ($k = 0, 1, 2, 3, \ldots$) and are zero otherwise. One can see from Eqs. (5) that increasing the number of discrete levels N increases a_1, c_1, e_1, and g_1 toward unity and decreases b_1, d_1, f_1, and h_1 toward zero. Moreover, as the number of discrete levels increases, the higher-order terms tend to reach zero as well; thus, at the limit of an infinite number of discrete levels, Eq. (4) degenerates to the case of a continuous space-variant subwavelength grating.[9]

With the use of Fourier analysis, the first coefficients of Eq. (4) yield

$$AS_0 + \frac{1}{2}(A + C)S_1 = \frac{4}{d} \int_0^d S_0'(x)\mathrm{d}x, \tag{6a}$$

$$B(S_1 + S_0)a_1 + (BS_2 - DS_3)b_1 = \frac{8}{d} \int_0^d S_0'(x) \cos\left(\frac{2\pi x}{d}\right)\mathrm{d}x, \tag{6b}$$

$$(BS_2 - DS_3)a_1 + B(S_1 + S_0)b_1 = \frac{8}{d} \int_0^d S_0'(x) \sin\left(\frac{2\pi x}{d}\right)\mathrm{d}x, \tag{6c}$$

$$(A - C)(S_1 e_1 + S_2 f_1) = \frac{16}{d} \int_0^d S_0'(x) \cos\left(\frac{4\pi x}{d}\right)\mathrm{d}x, \tag{6d}$$

$$(A - C)(S_1 f_1 + S_2 e_1) = \frac{16}{d} \int_0^d S_0'(x) \sin\left(\frac{4\pi x}{d}\right)\mathrm{d}x. \tag{6e}$$

These equations are a linear combination of the Stokes parameters of the incident beam. To extract S_0–S_3, Eqs. (6) should represent four independent equations, which are obtained for $N \geqslant 5$. However, a larger number of discrete levels N is desirable, in which case a larger portion of the intensity is represented by the first harmonics of every series of Eq. (4) and therefore a larger signal-to-noise ratio can be obtained. We note that the grating coefficients A, B, C, and D should be determined by direct measurement of the subwavelength grating parameters t_x, t_y, and ϕ or by performing a suitable calibration process. The full synthesis of the incoming polarization state is given in Appendix B. Moreover, an interesting physical insight into our polarimeter approach is given in Appendix A by use of Jones calculus.

3. REALIZATION PROCEDURE AND EXPERIMENTAL RESULTS

The DSG element for CO_2 laser radiation of 10.6-μm wavelength was fabricated upon a 500-μm-thick GaAs wafer with $\Lambda = 2\ \mu$m, $d = 2.5$ mm, and $N = 16$. The dimensions of the element were 30 mm $\times$ 3 mm and consisted of 12 periods of d. First, a binary chrome mask of the grating was fabricated by using high-resolution laser lithography. The pattern was then transferred onto the GaAs wafer by use of photolithography, after which we etched the grating by electron cyclotron resonance with

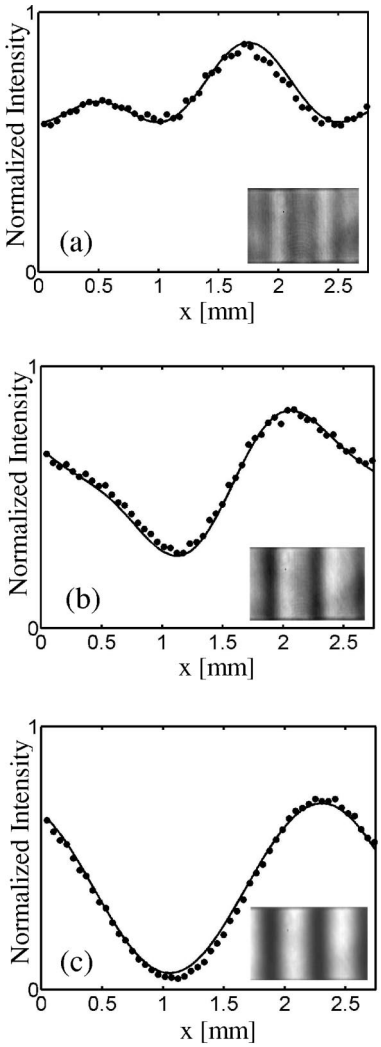

Fig. 3. Measured (circles) and predicted (solid curves) values of the normalized transmitted intensity as a function of the x coordinate along the DSG when the fast axis of the rotating QWP was at angles (a) 0°, (b) 20°, and (c) 45°; the insets show the experimental images of the near-field transmitted intensities.

BCl_3 for 35 min, resulting in an approximately 2.5-μm groove depth. Finally, an antireflection coating was applied to the back side of the wafer. Figure 2(c) shows a scanning electron microscopy image of a region on the subwavelength structure that we fabricated, whereas Fig. 2(d) depicts an image of a cross section of the subwavelength grooves.

Following the measurements, we used the setup depicted in Fig. 1 to test our concept for polarization measurements, whereby a subwavelength metal wire grating was used as a polarizer.[10] First, a calibration process was performed by illuminating the DSG followed by a polarizer with horizontal, vertical, and right-hand circularly polarized light. We determined the experimental optical parameters by fitting the curve of Eq. (4) to the measured intensity distributions, using a least-mean-squares algorithm, with t_x, t_y, and ϕ of the DSG as free parameters. The calibration process yielded a DSG having $t_x = 0.9$, $t_y = 0.8$, and retardation $\phi = 0.3\pi$ rad. These values are close both to the theoretical predictions of $t_x = 0.87$, $t_y = 0.81$, and $\phi = 0.352\pi$ rad that were achieved by using a rigorous coupled-wave analysis[12] for a groove profile depicted in Fig. 2(d) and to the direct measurement of the optical parameters using ellipsometric techniques,[6] which resulted in $t_x = 0.940$, $t_y = 0.833$, and $\phi = 0.281\pi$ rad with a standard deviation of approximately 0.02 for t_x and t_y and of 0.022 rad for ϕ. We found that in our etching process, the errors in the etching depth were approximately 5% of the nominal depth (3.3 μm). Therefore we can relate the deviations of t_x, t_y, and ϕ to the spatial errors in the etching process. Note that the calibration values also take into account other imperfections of the optical setup.

To test the ability of our device in conducting polarization measurements of fully polarized light, we used a CO_2 laser that emitted linearly polarized light at a wavelength of 10.6 μm and replaced the polarization-sensitive medium with a QWP. The images were captured by a Spiricon Pyrocam III 124 × 124 two-dimensional pyroelectric detection array at a rate of 24 Hz. Figure 3 shows the

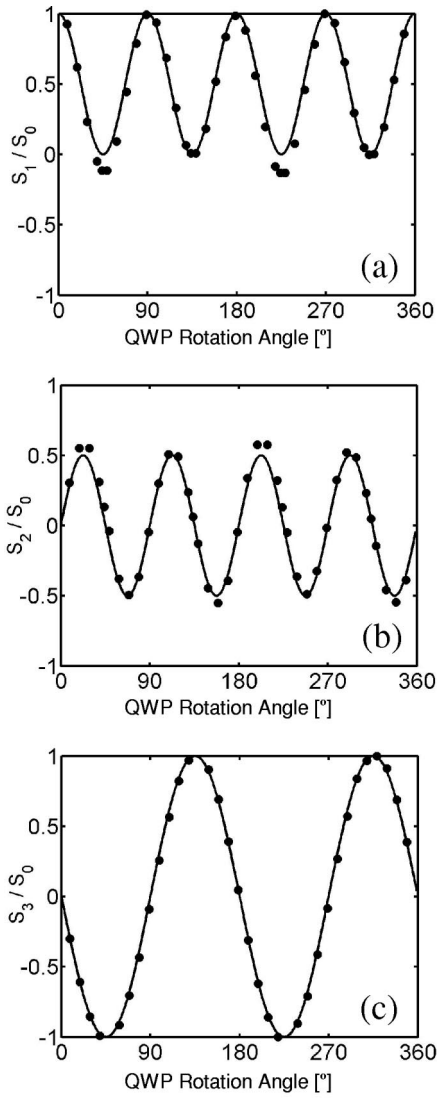

Fig. 4. Measured (circles) and predicted (solid curves) values of the normalized Stokes parameters (a) S_1/S_0, (b) S_2/S_0, and (c) S_3/S_0 as a function of the orientation of the QWP.

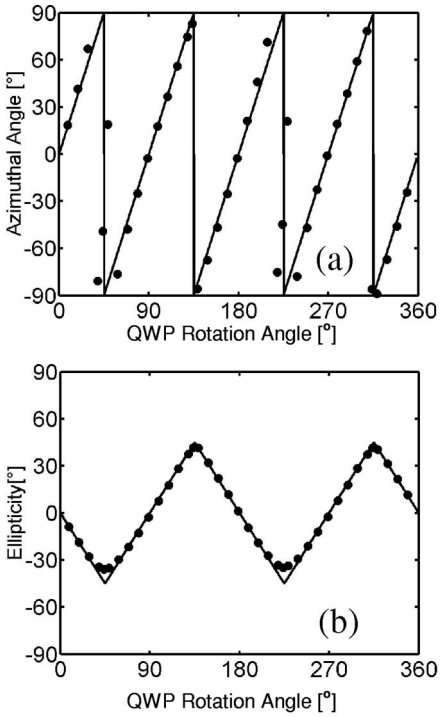

Fig. 5. Measured (circles) and predicted (solid curves) values for (a) azimuthal angle ψ and (b) ellipticity angle χ as a function of orientation of the QWP.

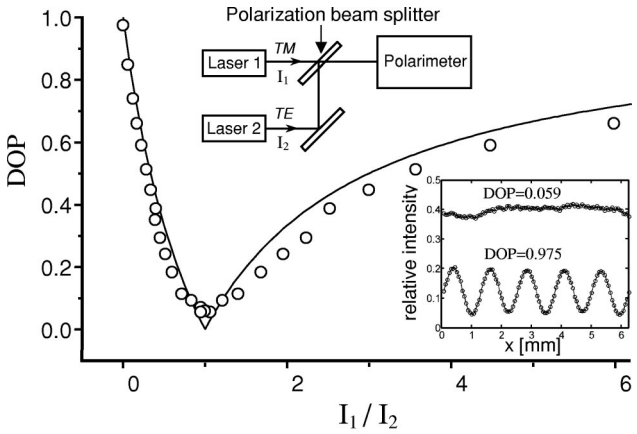

Fig. 6. Calculated (solid curve) and measured (circles) DOP as a function of intensity ratio of the two independent lasers having orthogonal linear polarization states, as used in a setup depicted in the top inset. The bottom inset shows calculated (solid curves) and measured (circles) intensity cross sections for the two extremes, $I_1 = I_2$ (DOP = 0.059) and $I_2 = 0$ (DOP = 0.975).

measured intensity distributions captured in a single camera frame, when the fast axis of the QWP was set at angles 0°, 20°, and 45°, as well as the predicted results. The prediction was obtained by inserting the expected values for the incoming Stokes parameters into Eq. (4) for $A = 1.45, B = 0.17, C = 0.8464$, and $D = 1.165$. Consequently, Fig. 4 shows the measured and predicted Stokes parameters of a resulting beam as a function of the orientation of the QWP. We determined the experimental values of S_1, S_2, and S_3 by using Eqs. (B1a)–(B1d). The integrals α, β, γ, and δ were numerically evaluated from the acquired data by using the Simpson algorithm. There is a good agreement between the predictions and the experimental results. Moreover, Fig. 5 shows the experimental and theoretical azimuthal angle ψ and the ellipticity angle χ, calculated from the data in Fig. 4, by use of the relations $\tan(2\psi) = S_2/S_1$ and $\sin(2\chi) = S_3/S_0$.[6] The measurements yield a standard deviation error with respect to the theoretical predictions of 2.6° and 0.6° for the azimuthal angle and the ellipticity angle, respectively. The errors of the polarization measurements result mainly from systematic errors such as the nature of the algorithm, imprecision in the rotation of the QWP, spatial inhomogeneity in the QWP retardation, which is approximately ±2°, spatial inhomogeneity in the retardation of the subwavelength grating, which is approximately ±1.3° (8% of the nominal phase), and low resolution of the IR camera and dynamic range, as well as statistical noise due to spatial and temporal fluctuation of the light emitted from the laser, shot noise and amplifier noise of the IR camera, pixel response nonuniformity, and quantization noise. The standard deviations in the azimuthal angle and the ellipticity angle for a series of successive measurements were 0.2° and 0.07°, respectively.

To demonstrate the use of a DSG for polarimetry of partially polarized beams, we combined two independent CO_2 lasers of orthogonal linear polarization states by use of the setup depicted in the inset at the top of Fig. 6. The degree of polarization (DOP) is defined by $\mathrm{DOP} = ({S_1}^2 + {S_2}^2 + {S_3}^2)^{1/2}/S_0$. For incoherent beam summation, the Stokes vector of the resulting beam is the sum of the Stokes vectors of the combined beams.[6] In the case of two orthogonal linearly polarized beams, the DOP is given by $\mathrm{DOP} = (I_1 - I_2)/(I_1 + I_2)$, where I_1 and I_2 are the intensities of the horizontally and vertically polarized beams, respectively. Figure 6 shows the measured and predicted DOP as a function of the intensity ratio I_1/I_2. The inset shows the experimental intensity distributions for two extreme cases. The first is for equal intensities ($I_1 = I_2$), in which the measured DOP is 0.0059, indicating unpolarized light. The second is for illumination of a single laser only (i.e., $I_2 = 0$), in which the measured DOP is 0.975, indicating fully polarized light. This experiment shows the ability to obtain all four Stokes parameters simultaneously, thereby emphasizing the good agreement between prediction and measurement for partially polarized light.

4. CONCLUSIONS

We have theoretically analyzed and experimentally demonstrated the use of a computer-generated space-variant discrete subwavelength dielectric grating for real-time polarization measurement. The discrete subwavelength gratings are unlimited in their dimensions, have uniform optical properties (t_x, t_y, and ϕ), and, in general, are lightweight, compact, and highly efficient. Both the space-variant subwavelength dielectric grating and the polarizer were realized by using photolithographic techniques commonly used in the production of microelectric devices. Therefore the camera and the gratings could be combined into a single chip, resulting in a very small device for polarization measurements.

APPENDIX A: THEORETICAL ANALYSIS FROM THE INTERFERENCE POINT OF VIEW

Subwavelength quasi-periodic structures are conveniently described as depicted in Fig. 2 by using Jones calculus. The analysis in this case is limited to fully polarized coherent beams. The DSG, which is a birefringent element with optical axes (parallel and perpendicular to the grating grooves) that rotate periodically in the x direction, can be represented as a polarization diffraction grating. When a plane wave with a uniform polarization is incident upon such a periodic subwavelength structure, the transmitted field will be periodic in both the polarization state and the phase front; therefore we can expect this field to yield discrete diffraction orders. The interference between the diffraction orders in the near field yields spatial intensity modulation. Evidently, the resulting interferogram pattern is directly related to the incident polarization state.

In this representation a uniform periodic subwavelength structure, the grooves of which are oriented along the y axis, can be described by the Jones matrix

$$\mathbf{J} = \begin{bmatrix} t_x & 0 \\ 0 & t_y \exp(i\phi) \end{bmatrix}, \tag{A1}$$

where t_x and t_y are the real amplitude transmission coefficients for light polarized perpendicular and parallel to the optical axes and ϕ is the retardation of the grating. Consequently, the space-dependent transmission matrix of the DSG can be described by

$$\mathbf{T}_C(x) = \mathbf{M}(\theta(x))\mathbf{J}\mathbf{M}^{-1}(\theta(x)), \tag{A2}$$

where $\theta(x)$ is the discrete local orientation of the optical axis given by Eq. (3) and Fig. 2(b), and $\mathbf{M}(\theta) = \left[\begin{smallmatrix} \cos\theta & -\sin\theta \\ \sin\theta & \cos\theta \end{smallmatrix}\right]$ is the two-dimensional rotation matrix. Note that, meanwhile, the polarizer is omitted from the optical system, and this will be referred to below.

For convenience, we convert $\mathbf{T}_C(x)$ to the helicity basis; therefore the space-variant polarization grating can be described by the matrix $\mathbf{T}(x) = \mathbf{U}\mathbf{T}_C\mathbf{U}^{-1}$, where $\mathbf{U} = 1/\sqrt{2}\left[\begin{smallmatrix} 1 & 1 \\ -i & i \end{smallmatrix}\right]$ is a unitary conversion matrix. Explicit calculation of $\mathbf{T}(x)$ yields

$$\mathbf{T}(x) = \frac{1}{2}[t_x + t_y \exp(i\phi)]\begin{bmatrix} 1 & 0 \\ 0 & 1 \end{bmatrix} + \frac{1}{2}[t_x - t_y \exp(i\phi)] \times \begin{bmatrix} 0 & \exp[i2\theta(x)] \\ \exp[-i2\theta(x)] & 0 \end{bmatrix}. \tag{A3}$$

We further adopt the Dirac bra–ket notation, in which $|\mathbf{R}\rangle = (1, 0)^{\mathrm{T}}$ and $|\mathbf{L}\rangle = (0, 1)^{\mathrm{T}}$ are the two-dimensional unit vectors for right-hand and left-hand circularly polarized light, respectively. Thus the resulting field is the product of an incident plane wave with arbitrary polarization $|\mathbf{E}_{\mathrm{in}}\rangle$ and the space-dependent transmission matrix $\mathbf{T}(x)$ given by Eq. (A3), yielding

$$|\mathbf{E}_{\mathrm{out}}\rangle = \eta_E|\mathbf{E}_{\mathrm{in}}\rangle + \eta_R \exp[i2\theta(x, y)]|\mathbf{R}\rangle + \eta_L \exp[-i2\theta(x, y)]|\mathbf{L}\rangle, \tag{A4}$$

where

$$\eta_E = \tfrac{1}{2}[t_x + t_y \exp(i\phi)],$$

$$\eta_R = \tfrac{1}{2}[t_x - t_y \exp(i\phi)]\langle\mathbf{E}_{\mathrm{in}}|\mathbf{L}\rangle,$$

$$\eta_L = \tfrac{1}{2}[t_x - t_y \exp(i\phi)]\langle\mathbf{E}_{\mathrm{in}}|\mathbf{R}\rangle$$

are the complex field coefficients and $\langle\alpha|\beta\rangle$ denotes the inner product. From Eq. (A4) it is evident that the emerging beam from the DSG, which is denoted by $|\mathbf{E}_{\mathrm{out}}\rangle$, comprises three polarization orders. The first maintains the original polarization state and phase of the incident beam, the second is right-hand circularly polarized with a phase modification of $2\theta(x)$, and the third has polarization direction and phase modification opposite to those of the former polarization order. Note that the phase modification of the $|\mathbf{R}\rangle$ and $|\mathbf{L}\rangle$ polarization orders results solely from local changes in the polarization state and therefore is geometrical in nature.[13]

Since $\theta(x)$ is a periodic function [Eq. (3), Fig. 2(b)], the functions $\exp[i2\theta(x)]$ and $\exp[-i2\theta(x)]$ in Eq. (A4) can be expanded into a Fourier series. Taking into account the connection between the Fourier series of the conjugated functions $\exp[i2\theta(x)]$ and $\exp[-i2\theta(x)]$ leads to the equation

$$|\mathbf{E}_{\mathrm{out}}\rangle = \eta_E|\mathbf{E}_{\mathrm{in}}\rangle + \eta_R \sum_{m=-\infty}^{\infty} \alpha_m \exp(i2\pi mx/d)|\mathbf{R}\rangle + \eta_L \sum_{m=-\infty}^{\infty} \alpha_{-m}^{*} \exp(i2\pi mx/d)|\mathbf{L}\rangle, \tag{A5}$$

where $\alpha_m = (2/d)\int_0^d \exp\{i2[\theta(x) + m\pi x/d]\}\mathrm{d}x$. Based on Eq. (A5), we find that the diffraction efficiency into the mth diffracted order of the $|\mathbf{R}\rangle$ polarization order ($\eta_m^R = |\alpha_m|^2$) is equal to the diffraction efficiency into the $-m$th diffracted order of $|\mathbf{L}\rangle$ ($\eta_{-m}^L = |\alpha_m^*|^2$); thus $|\mathbf{R}\rangle$ and $|\mathbf{L}\rangle$ diffract in opposite manners. Therefore, as depicted in Fig. 7, once a uniformly polarized beam is incident upon the DSG, the resulting beam comprises three polarization states described by Eq. (A4), whereas the polarization orders of $|\mathbf{R}\rangle$ and $|\mathbf{L}\rangle$ states are split into multiple diffraction orders as a result of the discontinuity of the phase, $2\theta(x)$.

In our near-field polarimetry concept, the wave front emerging from the polarization grating is incident upon a linear polarizer, described in the helicity basis by a Jones matrix of the form

$$\mathbf{P} = \frac{1}{2}\begin{bmatrix} 1 & 1 \\ 1 & 1 \end{bmatrix}.$$

The linearly polarized field emerging from the polarizer is given by the product of Eq. (A5) and P, yielding

$$\tilde{E}_{\mathrm{out}} = \frac{1}{\sqrt{2}}\left[\eta_E(\langle E_{\mathrm{in}}|R\rangle + \langle E_{\mathrm{in}}|L\rangle) + \eta_R \sum_{m=-\infty}^{\infty} \alpha_m \exp(i2\pi mx/d) + \eta_L \sum_{m=-\infty}^{\infty} \alpha_{-m}^{*} \exp(i2\pi mx/d)\right]. \tag{A6}$$

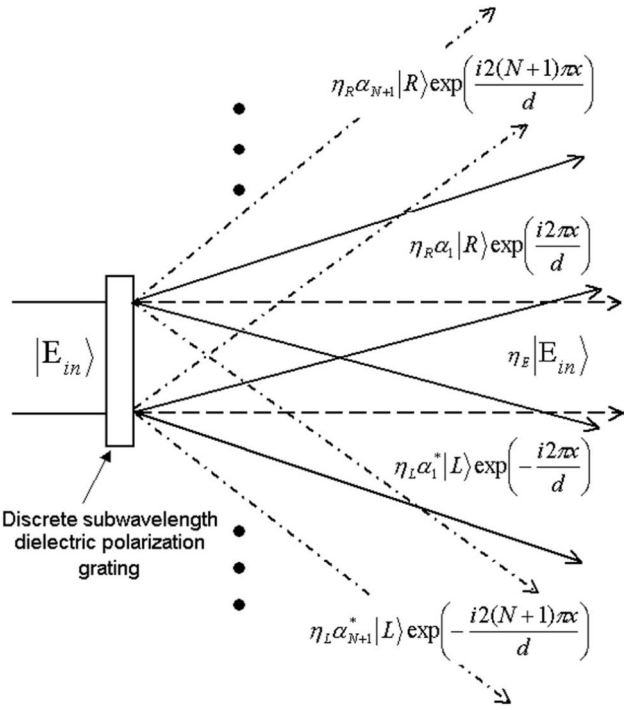

Fig. 7. Diffraction orders emerging from the DSG: zero order (dashed), first order for $|\mathbf{R}\rangle$ and $|\mathbf{L}\rangle$ polarized beams (solid), and higher order for $|\mathbf{R}\rangle$ and $|\mathbf{L}\rangle$ polarized beams (dotted–dashed).

Consequently, the intensity distribution is given by $|\tilde{E}_{\text{out}}|^2$, which results, after some algebraic manipulations, in an expression identical to that given in Eq. (4).

Note that if we use a 4-f telescope configuration for imaging the emerging beam from our polarimeter and insert a spatial filter in the Fourier plane, the higher diffracted orders can be eliminated. Therefore this can result in an intensity distribution resembling the pattern obtained by the continuous-grating-based polarimeter.[9]

APPENDIX B: SYNTHESIS OF THE INCOMING POLARIZATION STATE AS A FUNCTION OF THE MEASURED INTENSITY

In this appendix we show the full synthesis of the incoming polarization state as a function of the measured intensity by solving Eqs. (6a)–(6e). Only four equations are required to fully determine the polarization state, whereas the possible choice of equations depends on the number of discrete levels N. However, for $N > 8$ any four equations out of the given five is suitable. From our evaluation the best results could be obtained by omitting Eq. (6b). The remaining equations can be written in matrix form as $\mathbf{HS} = \mathbf{R}$, where $\mathbf{S} = (S_0, S_1, S_2, S_3)^{\mathrm{T}}$ is the incoming polarization state, $\mathbf{R} = (\alpha, \beta, \gamma, \delta)^{\mathrm{T}}$, and $\mathbf{H}$ is the coefficient matrix. Explicitly, α, β, γ, and δ are given by

$$\alpha = \frac{4}{d}\int_0^d S_0'(x)\mathrm{d}x, \qquad \beta = \frac{8}{d}\int_0^d S_0'(x)\sin(2\pi x/d)\mathrm{d}x,$$

$$\gamma = \frac{16}{d}\int_0^d S_0'(x)\cos(4\pi x/d)\mathrm{d}x,$$

$$\delta = \frac{16}{d}\int_0^d S_0'(x)\sin(4\pi x/d)\mathrm{d}x,$$

whereby the coefficient matrix is

$$\mathbf{H} = \begin{bmatrix} A & (A+C)/2 & 0 & 0 \\ Bb_1 & Bb_1 & Ba_1 & -Da_1 \\ 0 & (A-C)e_1 & (A-C)f_1 & 0 \\ 0 & (A-C)f_1 & (A-C)e_1 & 0 \end{bmatrix}.$$

We note that the coefficients A,B,C, and D could be determined from a suitable calibration process. In that case $\mathbf{H}$ is fully known by use of Eqs. (5). Consequently, the incoming polarization state can be calculated, by using Kramer's method, to yield

$$S_0 = \frac{1}{A}\left(\alpha - \frac{1}{2}\frac{A+C}{A-C}\frac{\gamma e_1 - \delta f_1}{{e_1}^2 - {f_1}^2}\right), \tag{B1a}$$

$$S_1 = \frac{1}{A-C}\frac{\gamma e_1 - \delta f_1}{{e_1}^2 - {f_1}^2}, \tag{B1b}$$

$$S_2 = \frac{1}{A-C}\frac{\delta e_1 - \gamma f_1}{{e_1}^2 - {f_1}^2}, \tag{B1c}$$

$$S_3 = \frac{1}{Da_1}\left\{-\beta + \frac{B}{A}b_1\alpha + \frac{B}{({e_1}^2 - {f_1}^2)} \times \left[\left(\frac{b_1e_1}{2A} + \frac{a_1f_1}{A-C}\right)\gamma - \left(\frac{b_1f_1}{2A} + \frac{a_1e_1}{A-C}\right)\delta\right]\right\}. \tag{B1d}$$

REFERENCES

1. J. Lee, J. Koh, and R. W. Collins, "Multichannel Mueller matrix ellipsometer for real-time spectroscopy of anisotropic surfaces and films," Opt. Lett. **25**, 1573–1575 (2000).
2. V. Sankaran, M. J. Everett, D. J. Maitland, and J. T. Walsh, Jr., "Comparison of polarized light propagation in biological tissue and phantoms," Opt. Lett. **24**, 1044–1046 (1999).
3. G. P. Nordin, J. T. Meier, P. C. Deguzman, and M. W. Jones, "Micropolarizer array for infrared imaging polarimetry," J. Opt. Soc. Am. A **16**, 1168–1174 (1999).
4. P. C. Chou, J. M. Fini, and H. A. Haus, "Real-time principle state characterization for use in PMD compensators," IEEE Photon. Technol. Lett. **13**, 568–570 (2001).
5. G. E. Jellison, Jr., "Four channel polarimeter for time-resolved ellipsometry," Opt. Lett. **12**, 766–768 (1987).
6. E. Collet, *Polarized Light* (Marcel Dekker, New York, 1993).
7. R. M. A. Azzam, "Integrated polarimeters based on anisotropic photodetectors," Opt. Lett. **12**, 555–557 (1987).
8. F. Gori, "Measuring Stokes parameters by means of a polarization grating," Opt. Lett. **24**, 584–586 (1999).
9. Z. Bomzon, G. Biener, V. Kleiner, and E. Hasman, "Real-time analysis of partially polarized light with a space-variant subwavelength dielectric grating," Opt. Lett. **27**, 188–190 (2002).
10. Z. Bomzon, V. Kleiner, and E. Hasman, "Space-variant polarization state manipulation with computer-generated

subwavelength metal stripe gratings," Opt. Commun. **192**, 169–181 (2001).
11. P. C. Deguzman and G. P. Nordin, "Stacked subwavelength gratings as circular polarization filters," Appl. Opt. **40**, 5731–5737 (2001).
12. P. Lalanne and G. M. Morris, "Highly improved convergence of the coupled-wave method for TM polarization," J. Opt. Soc. Am. A **13**, 779–784 (1996).
13. E. Hasman, V. Kleiner, G. Biener, and A. Niv, "Polarization dependent focusing lens by use of quantized Pancharatnam–Berry phase diffractive optics," Appl. Phys. Lett. **82**, 328–330 (2003).